

Panoramic Distortion-Aware Tokenization for Person Detection and Localization in Overhead Fisheye Images

Nobuhiko Wakai¹ Satoshi Sato¹ Yasunori Ishii¹ Takayoshi Yamashita²

¹ Panasonic Holdings Corporation ² Chubu University

{wakai.nobuhiko,sato.satoshi,ishii.yasunori}@jp.panasonic.com

takayoshi@isc.chubu.ac.jp

Abstract

Person detection in overhead fisheye images is challenging due to person rotation and small persons. Prior work has mainly addressed person rotation, leaving the small-person problem underexplored. We remap fisheye images to equirectangular panoramas to handle rotation and exploit panoramic geometry to handle small persons more effectively. Conventional detection methods tend to favor larger persons because they dominate the attention maps, causing smaller persons to be missed. In hemispherical equirectangular panoramas, we find that apparent person height decreases approximately linearly with the vertical angle near the top of the image. Using this finding, we introduce panoramic distortion-aware tokenization to enhance the detection of small persons. This tokenization procedure divides panoramic features using self-similar figures that enable the determination of optimal divisions without gaps, and we leverage the maximum significance values in each tile of the token groups to preserve the significance areas of smaller persons. We propose a transformer-based person detection and localization method that combines panoramic-image remapping and the tokenization procedure. Extensive experiments demonstrated that our method outperforms conventional methods on large-scale datasets.

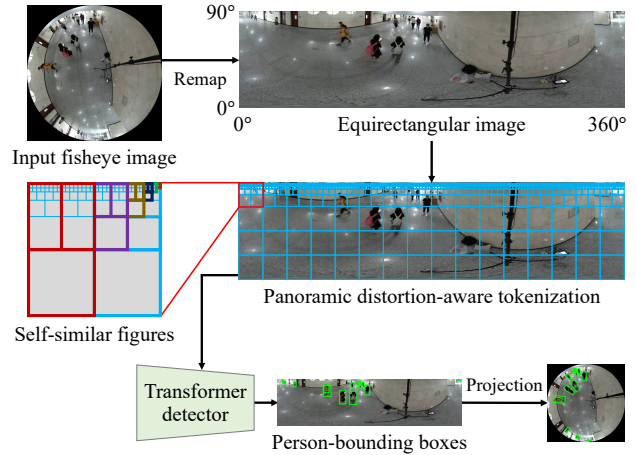


Figure 1. Our method converts an overhead fisheye image into an equirectangular image by remapping. To leverage the significance areas of smaller persons, a distortion-aware tokenization process based on a self-similar figure using a unit figure, which is colored dark red and consists of a square and two rectangles. Our transformer-based detector uses the resulting tokens to detect bounding boxes within the panoramic image, and then the boxes project to the fisheye image. The input image is taken from [65].

1. Introduction

Object detection methods are used in a wide range of applications in both the commercial and industrial fields, including visual surveillance [11, 26, 63, 68], pedestrian detection [7, 22, 71], and robotics [24, 66, 70]. In particular, the interest in fisheye image-based person detection has been growing because of its varied applications, which include monitoring of public transportation and infrastructure, worker movement optimization in factories, and player movement analysis for use in sports strategy. Overhead fisheye cameras are suitable for use in these applications

because they are omnidirectional and have a larger field of view than conventional narrow-view cameras; *i.e.*, one overhead fisheye camera can substitute for several narrow-view cameras. However, the overhead fisheye images do not match the inputs of the detectors [13, 18, 60, 69, 75], which require perspective images. This mismatch is derived from person rotation and from the presence of small persons in the images. The person rotation factor leads to individual persons having various shapes and appearances in the fisheye images. Within the near image circle of circumferential fisheye images, smaller people are captured at a long distance from the fisheye cameras. Although person detection methods based on use of narrow-view cameras are well-established, deriving accurate techniques for person detection and localization from overhead fisheye images has remained an open challenge.

Table 1. Comparison of the features of conventional methods with those of our proposed method

Method	Detector ¹	Training on overhead fisheye images	Bounding box	Core idea to address	
				Person rotation	Small person
CNN-based					
Seidel <i>et al.</i> [43]	VISAPP'19	YOLOv2 [37]	Orthogonal rectangle	✓	
Li <i>et al.</i> [25]	AVSS'19	YOLOv3 [38]	Rotated rectangle	✓	
Tamura <i>et al.</i> [50]	WACV'19	YOLOv2 [37]	Rotated rectangle	✓	
RAPiD [10]	CVPRW'20	FPN [28]	Rotated rectangle	✓	
OARPD [35]	MTA'24	YOLOv8m [55]	Rotated rectangle	✓	
Transformer-based					
Yang <i>et al.</i> [65]	ICCV'23	DAB-DETR [30]	Rotated rectangle	✓	
Ours		DAB-DETR [30]	Rotated trapezoid	✓	✓

¹ Each detector was modified to address overhead fisheye images. FPN represents feature pyramid networks.

Person detection methods have been proposed that used convolutional neural networks (CNNs) [23] and transformers [56] in overhead fisheye images. Early CNN-based methods [25, 43] used detectors that were trained on perspective images. To improve the performance of the CNN-based methods [10, 35, 50] and a transformer-based method [65], their training was also conducted using overhead fisheye images. However, it is difficult for these methods to detect persons accurately in overhead fisheye images because of the rotation and small-person problems.

On the basis of the observations above, to realize accurate person detection, we propose a transformer-based method that detects rotated bounding boxes from an overhead fisheye image, as illustrated in Figure 1. An input fisheye image is converted into a panoramic image using a remapping method. For the panoramic image, we introduce a tokenization method called panoramic distortion-aware tokenization (PDAT) to balance the significance areas of feature maps regardless of person sizes. This tokenization uses self-similar figures to perform nonuniform divisions while maintaining consistent person-to-tile size ratios, based on our finding that person height depends on the vertical image coordinates of the panoramic image. Finally, we obtain bounding boxes in the fisheye images via projection.

To investigate the effectiveness of these proposed methods, we conducted extensive experiments on three large-scale datasets [10, 51, 65]. This evaluation demonstrated that our proposed method outperforms both the conventional CNN-based [10, 25, 35, 43, 50] and transformer-based [65] methods. The major contributions of our study are summarized as follows:

- We propose a transformer-based method for person detection and localization in overhead fisheye images that achieves higher accuracy than conventional methods by balancing significance areas of the feature maps.
- We introduce the PDAT method with optimal divisions based on self-similar figures to address a person’s height using the vertical panoramic-image coordinates.
- We demonstrate the effectiveness of our proposed method by applying it to the challenging LOAF dataset. The aver-

age precision for distant person positions when using our method on the LOAF test set is substantially greater than that of the existing state-of-the-art method by 32.0.

2. Related work

Overhead-fisheye-image person detection. Person detection techniques in overhead fisheye images have been developed using various datasets [5, 10, 25, 51, 65]. Existing person detection methods for overhead fisheye images can be classified into two categories: CNN-based and transformer-based methods, as listed in Table 1. Seidel *et al.* [43] proposed a pioneering CNN-based detection method. The method divides a fisheye image into upright image patches that are undistorted using the given camera parameters. Although these patches are perspective images, the method requires camera calibration before detection. Li *et al.* [25] proposed a CNN-based method to improve detection accuracy using focal windows that can extract upright images. Tamura *et al.* [50] proposed a method that uses YOLOv2 [37], which had been trained on perspective images from the COCO dataset [27] using rotation augmentation. To train a detector called RAPiD, Duan *et al.* [10] introduced the angle-aware loss function. Inspired by RAPiD being trained on fisheye images, OARPD [35] was proposed with use of the center distance intersection over union approach to address rotated bounding boxes. Yang *et al.* [65] proposed a pioneering transformer-based method with rotation-equivariant training. For a query-based detector, this training strategy involves use of an additional query of a 90°-rotated image to tackle rotated persons. Both the CNN-based and transformer-based methods described above focused primarily on person rotation. Although the CNN-based and transformer-based methods can detect persons, images containing persons of various sizes cause performance degradation.

Small object detection. Object detection accuracy tends to decrease for smaller objects. Small objects are often captured at long distances, *e.g.*, in a dataset acquired using drones [74]. Small object detection methods are generally classified into four categories: division-based methods,

augmentation-based methods, enlargement-based methods, and spectrum-based methods. The division-based methods involve multi-scale training performed using image pyramids [46], image cropping [47], and feature pyramids [15]. The augmentation-based methods [13, 67] were proposed to realize data invariance. The enlargement-based methods enlarge the input images [29, 54, 59] and conduct super-resolution processing [20, 45]. The spectrum-based methods enhance the discrimination of objects from a frequency perspective [49]. The methods noted above do not use the prior knowledge that smaller persons are only located near the image circles in overhead fisheye images. Therefore, these conventional methods do not work effectively for person detection in overhead fisheye images.

Transformer tokenization. Dosovitskiy *et al.* [9] proposed a pioneering transformer-based method using a tokenization approach that divides an input image into square patches. Numerous tokenization methods have been proposed to date because these square patches lead to high computational costs. Window-based methods focus on the token groups using shifted windows [31], cross-shaped windows [8], dilated windows [53, 61], and scalable sliding windows [17]. In contrast to static window shapes, deformable attention methods [62] were proposed to improve flexibility. To address the problem of multiple tokens being generated in unimportant areas, *e.g.*, in the background, DynamicViT [36] and BiFormer [73] prune the areas, and SG-Former [39] aggregates the areas. Although the methods described above are all well-developed, these methods were designed for use with perspective images. For fisheye image applications, DarSwin [2], which uses radial patches formed by polar partitioning, was proposed. However, this partitioning approach is not suitable for overhead fisheye images because a small number of the relevant tokens are generated in near image circles.

Visual localization. Various localization methods have been established to determine either camera poses or person locations from an image. These methods can be classified into three categories: query-based methods, regression-based methods, and geometry-based methods. The query-based methods estimate camera poses using databases composed of geo-tagged images [1, 3, 19, 42, 52, 64] and 3D scene structure models [12, 41]. Before query-based methods can be used, the databases and models must first be built in a time-consuming process. The regression-based methods [21, 58] can estimate camera poses without the need for databases and models; however, their inferences can only be applied to the same scenes that were used for training. The geometry-based methods estimate horizontal distances of person positions based on the bounding boxes [65, 72] and head points [6] in overhead fisheye images. These geometry-based methods estimate person locations from image coordinates using camera parameters.

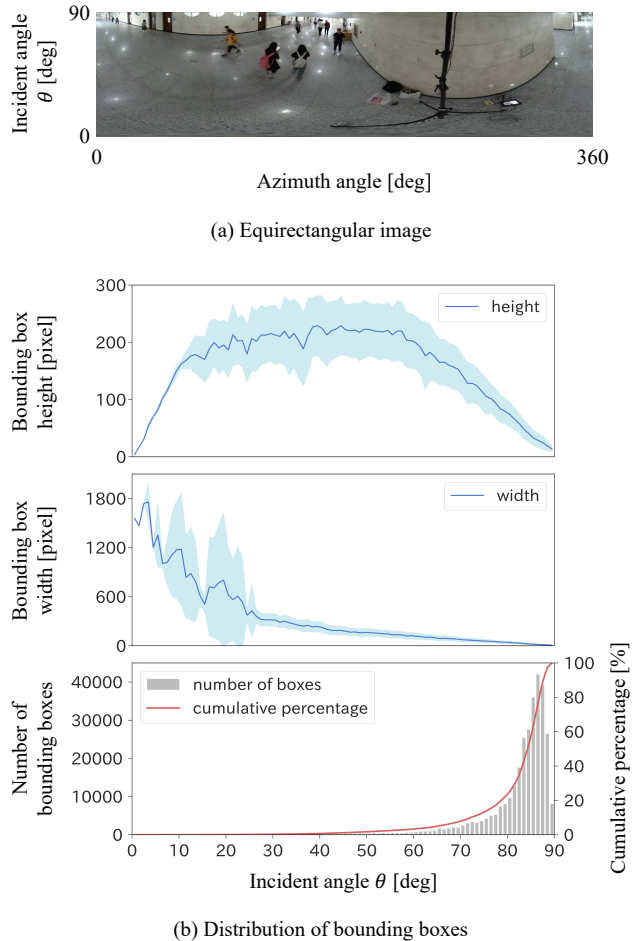


Figure 2. Analysis of overhead fisheye images. (a) An equirectangular image. The vertical and horizontal axes show the incident angle (0° is at the bottom of the image) and the azimuth angle, respectively. (b) Distribution of the bounding boxes in equirectangular images on the LOAF training set. This distribution was analyzed using incident angles θ at 1° -intervals based on the center of the bounding boxes. The top and middle panels represent the mean heights and widths of the bounding boxes in equirectangular images with 3072×768 pixels, respectively. The cyan areas indicate ± 1 standard deviations in each bin of incident angles. The bottom panel shows the number of bounding boxes.

3. Proposed method

First, we analyze the bounding boxes in an overhead fisheye image dataset. Second, we present the design of our method. Third, we introduce PDAT. Fourth, we describe our method using PDAT for person detection and localization. Finally, we describe our training and inference phases.

3.1. Geometric analysis of overhead fisheye images

We analyzed the LOAF training set [65] to understand the unique characteristics of overhead fisheye images, which

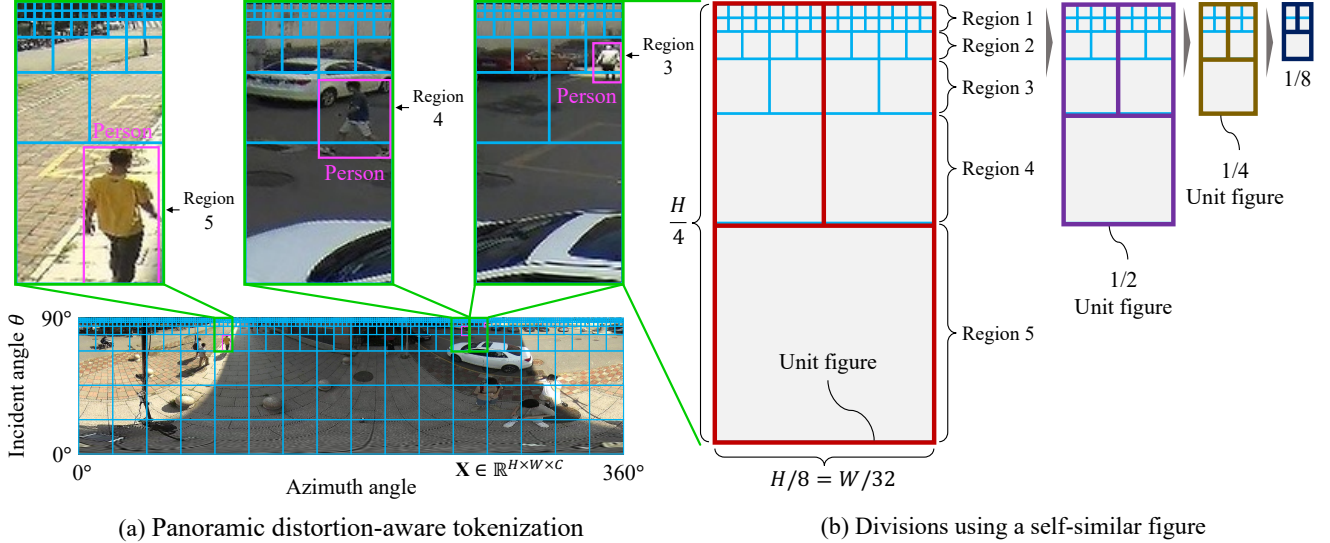


Figure 3. Panoramic distortion-aware tokenization. (a) A panoramic feature map is nonuniformly tiled with cyan grids along the incident-angle axis. The tile sizes are adjusted to match the person’s height in each region, maintaining similar person-to-tile size ratios across different regions. Enlarged views show person-bounding boxes in regions 3, 4, and 5. (b) A self-similar subdivision recursively partitions the unit figure and is truncated after three steps, yielding five regions ($K = 5$) with the size ratios of the unit figure: 1, $1/2$, $1/4$, and $1/8$.

differ from perspective images. We remapped overhead fisheye images to equirectangular images, as shown in Figure 2(a). A downward-looking fisheye camera observes the lower hemisphere, with incident angles θ ranging from 0° (nadir) to 90° (horizon). Figure 2(b) shows the distribution of bounding box heights and widths along different incident angles θ . Our analysis revealed two key findings:

- We found a geometric relationship between equirectangular images and overhead fisheye cameras: the heights and widths of person-bounding boxes decrease approximately linearly when the incident angles θ are large enough ($> 70^\circ$).
- We observed that 75% of all person-bounding boxes are concentrated in the range of incident angles from 80° to 90° , indicating a strong bias in person distribution.

This pattern in the first finding arises from the geometry of overhead fisheye cameras and is fundamentally different from that observed with perspective cameras, where object sizes primarily depend on distance. While the heights at smaller incident angles exhibit an upward-convex trend due to oblique viewing angles, we focus on the linear behavior at large incident angles, where the majority of bounding boxes are located, as indicated in the second finding.

Note that the bias in the second finding has two main causes. First, peripheral portions at large incident angles subtend larger ground areas. Second, due to motion parallax [14, 16], people farther from the camera exhibit smaller apparent image motion and remain in view longer, while nearer people traverse the field of view more quickly.

3.2. Design of our proposed method

We designed our proposed method based on the two key findings, as described in Section 3.1, because conventional detection methods, which assume uniform object distribution, may not be optimal for overhead fisheye images. The first finding suggests that our method uses the prior knowledge of the linear change in predictable bounding box sizes. The second finding indicates that focusing on bounding boxes with large incident angles is effective in terms of the number of bounding boxes. Conventional detectors allocate computation approximately uniformly across the image and do not explicitly exploit θ -dependent scale or distribution biases. Therefore, we designed our tokenization method to specifically account for these geometric relationships, focusing on the portions with large incident angles.

3.3. Panoramic distortion-aware tokenization

On the basis of the design discussed above, we propose PDAT that addresses person detection in overhead fisheye images. The key insight of PDAT is that it maintains consistent person sizes relative to tile sizes across different regions, regardless of their incident angles. To achieve this goal, PDAT employs nonuniform divisions that adapt to the varying sizes of persons at different incident angles, as shown in Figure 3(a). These tiles are designed to fill a panoramic feature map without gaps, ensuring complete coverage for reliable person detection.

As shown in Figure 2(b), the person’s height exhibits an approximately linear decrease at incident angles exceeding

70°. This portion corresponds to about the top quarter of the height of the equirectangular images. On the basis of this observation, we align square tiles whose sizes depend on the vertical axis. We found that use of consecutive half-sizes fills the feature maps, as illustrated in Figure 3(a). The top quarter of the image is occupied by performing consecutive half-size tiling, and the other three-quarters consist of tiles of uniform size because the bounding box heights show nonlinear trends in this region with fewer instances.

Each of these square tiles contains $a_k \times a_k$ feature vectors, where a_k represents the number of feature vectors along each side of a tile in the k th region, as shown in Figure 3(b). Our tiling is defined on the basis of the self-similar figures when using K regions, with the exception that the top two rows in region 1 have tiles of the same size due to finite divisions. The unit figure consists of a square and two rectangles, and each rectangle can be divided recursively using another set composed of a square and two rectangles, as illustrated in the rightmost part of Figure 3(b). Note that our division method was inspired by the Cantor ternary set [48], but our self-similar figure is not a fractal according to Mandelbrot’s definition [33].

Although the tile sizes vary among regions 3, 4, and 5, as shown in Figure 3(a), the person-bounding boxes appear similar in size relative to their respective tiles. This design maintains similar complexity across all regions, despite the varying absolute sizes of persons in the panoramic image. As illustrated in Figure 3(b), our tokenization method uses recursive divisions to maintain consistent person-to-tile size ratios, particularly in portions with large incident angles.

3.4. Network architecture

Our network architecture consists of four main components: panoramic image conversion, a detector head based on the dynamic anchor box detection with transformers (DAB-DETR) [30], a backbone based on SG-Former [39], and our proposed PDAT.

Panoramic image conversion. Our method converts an input fisheye image into an equirectangular panoramic image via remapping, as illustrated in Figure 4. When the input image is rectangular, we center-crop the image. To address any uncalibrated cameras, we assume that the input images represent the stereographic projection, which is a standard fisheye camera model. In the case of radial distortion [57], this projection uses a trigonometric function: $\gamma = 2f_w \cdot \tan(\theta/2)$, where γ is the distortion, f_w is the focal length, and θ represents the incident angle, as shown in Figure 2(a). We can then determine the focal length by fitting the image circle using 90° incident angles. The image coordinates in the fisheye images are projected onto a unit sphere in world coordinates using backprojection [57], and then the world coordinates are projected onto an equirectangular image with an arbitrary image width [44]. We use

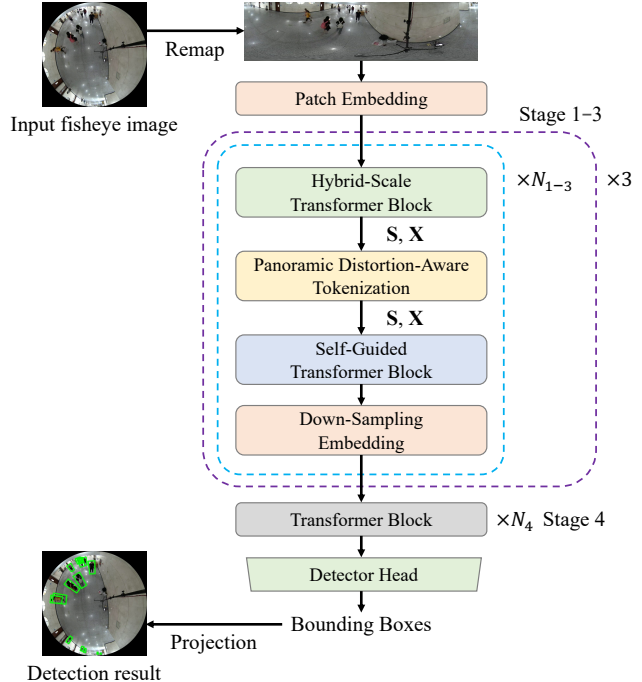


Figure 4. Overall network architecture of our proposed method. The model consists of a detector head and a backbone with four stages. The N in the subscript stage indicates the block count. The S and X are the significance map and feature map, respectively.

panoramic images with incident angles from 0° to 90° because the incident angle range from 90° to 180° represents the directions behind the cameras.

Detector and backbone selection. Following the approach in [65], we use DAB-DETR [30], which has shown strong object detection performances. Window-based transformers are not suitable for use in the backbone of DAB-DETR because PDAT divides the feature maps nonuniformly. Therefore, we use an aggregation-based transformer called SG-Former [39] for the backbone. Note that SG-Former is the only aggregation-based method of this type available. The proposed network architecture is shown in Figure 4. The detector head represents DAB-DETR without the backbone, and the remaining blocks represent SG-Former and PDAT. The patch embedding is extracted using the CNN, and the transformer block is a vanilla transformer block [9]. The implementations of DAB-DETR and SG-Former follow the details provided in their respective papers. We explain the integration of PDAT into SG-Former in the following two steps: 1) SG-Former attention mechanism and 2) PDAT integration details.

SG-Former attention mechanism. The core ideas of the SG-Former are hybrid-scale self-attention and self-guided attention. The hybrid-scale attention process extracts both global and local information from a feature map

$\mathbf{X} \in \mathbb{R}^{H \times W \times C}$, where H , W , and C are the height, the width, and the channels of the map, respectively. The hybrid-scale attention process also calculates the significance map $\mathbf{S} \in \mathbb{R}^{H \times W}$, based on the feature map. For example, the face is a high-significance area and the background is a low-significance area. The self-guided attention process aims to aggregate the feature vectors based on the significance map. For example, the feature vectors in a high-significance area of the face are aggregated into half the number of feature vectors; in contrast, the feature vectors in a low-significance area of the background are aggregated into 1/28th feature vectors. To obtain multi-scale features, down-sampling is applied between stages.

PDAT integration details. We aim to extend the self-guided attention process using PDAT. Our modification of SG-Former inserts PDAT between the hybrid-scale transformer block and the self-guided block, as shown in Figure 4. The PDAT method leverages the significance map \mathbf{S} based on the feature vectors grouped by the tiles. The integration process consists of the following steps. First, the significance maps are divided using our tiling method, as described in Section 3.3. From top to bottom, we split these maps horizontally into strips called regions, as shown in Figure 3(b). Second, we extract 2D max pooling indices for each region k using square kernels of $a_k \times a_k$ with horizontal strides a_k in each tile. The a_k corresponds to the height of region k in the upper quarter of the image, with the exception that region 1 uses its half height, while a fixed height of $H/4$ is used for the remaining three-quarters. Finally, we leverage the significance values extracted by the max pooling from the second step. In this leveraging, the significance values are multiplied by the scale factor α .

This approach seamlessly integrates into the self-guided attention procedure to preserve the significance values of smaller persons in the feature vector aggregation process. We introduce this scaling because larger persons dominate the attention mechanism by generating multiple high-significance areas in SG-Former without PDAT.

3.5. Training and inference

Training. We generate equirectangular images from each training set. In this generation procedure, we avoid splitting the bounding boxes in the vertical image edges by changing the definition of the 0° azimuth angles. We then train our network using the panoramic images by following [30].

Inference. First, we convert an input fisheye image into a panoramic image by a remapping process, as illustrated in Figure 4. Second, the remapped panoramic image is then fed into our network. Finally, we project the detected bounding boxes onto the fisheye image, on which the shape of each bounding box is a rotated trapezoid. This projection represents the backprojection from a fisheye image to a panoramic image.

4. Experiments

To demonstrate the validity and effectiveness of our approach, we conducted extensive experiments using three large-scale datasets [10, 51, 65], which are composed of overhead fisheye images. We used 1024×1024 input resolution by following the settings given in [10, 25, 43, 50, 65]. For evaluation, we converted the trapezoid bounding boxes into rectangles because no other methods listed in Table 1 produced trapezoid outputs.

4.1. Parameter settings

For our network backbone, we used SG-Former-S [39], which was pretrained on ImageNet [40]. The SG-Former-S, which has the smallest backbone size among S, M, and B types, is comparable to Swin Transformer-T [31] used in Yang *et al.*'s method [65]. We trained our network using a combination of a mini-batch size of 8 for 120 epochs and the AdamW optimizer [32]. The initial learning rate was set to 2×10^{-4} and was multiplied by 0.1 at the 40th epoch. We set the number of regions $K = 5$ and the scale factor $\alpha = 2$. Because the majority of bounding boxes were near the image circles of fisheye images, we adopted the 3072-pixel width of panoramic images, approximately corresponding to the circumference of fisheye images with 1024×1024 pixels: $\pi \times 1024 = 3217 \approx 3072$ pixels. Unless otherwise specified, we employed panoramic images with 3072×768 pixels.

4.2. Person localization

For person localization, we adopt the geometry-based method proposed by Yang *et al.* [65]. This method estimates person locations by calculating the intersection point between the incident ray from the camera and the ground plane, where the incident ray is determined from the center of the lower edge of a detected person-bounding box.

4.3. Experimental results

We used the person detection and localization results reported by Yang *et al.* [65] in the methods of Seidel *et al.* [43], Li *et al.* [25], Tamura *et al.* [50], RAPiD [10], and Yang *et al.* [65]. We also used the OARPD [35] results reported in [35]. Unless otherwise specified, we refer to these results throughout. Because of the lack of previous performance reports, we implemented methods for comparison of Tamura *et al.* [50] and OARPD [35], based on the corresponding papers using PyTorch [34]. In addition, the official codes from Yang *et al.* [65] and RAPiD [10] were used for evaluation.

4.3.1. Person detection on LOAF

Metrics and protocols. To demonstrate the validity and the effectiveness of the proposed method on LOAF, we used the

Table 2. Person detection results using the average precision (AP) \uparrow on the LOAF validation (val) and test sets

Method	val								test							
	mAP	AP ₅₀	AP ₇₅	AP _n	AP _m	AP _f	AP _{seen}	AP _{unseen}	mAP	AP ₅₀	AP ₇₅	AP _n	AP _m	AP _f	AP _{seen}	AP _{unseen}
Seidel <i>et al.</i> [43]	21.8	59.8	7.6	32.8	28.5	2.3	23.2	19.5	20.2	58.2	7.1	32.2	28.3	3.9	22.4	18.9
Li <i>et al.</i> [25]	28.5	63.3	20.1	46.8	24.2	1.3	33.8	29.3	27.2	65.2	21.3	47.2	24.8	1.3	31.8	27.6
Tamura <i>et al.</i> [50]	34.8	72.1	27.7	51.7	38.8	8.7	38.8	32.9	34.2	72.8	28.7	53.7	37.3	6.5	39.5	33.2
RAPiD [10]	40.3	77.9	34.8	55.3	41.9	9.2	44.7	37.6	39.2	77.9	35.4	54.8	40.1	7.9	44.2	37.3
OARPD [35]	45.5	78.8	46.3	-	-	-	-	-	45.8	79.4	45.8	-	-	-	-	-
Yang <i>et al.</i> [65]	47.4	82.6	48.4	64.1	54.3	14.1	50.8	45.7	46.2	81.1	47.3	66.1	53.5	12.6	49.3	44.9
Ours	52.4	84.6	57.6	66.3	57.9	42.9	56.3	50.7	54.5	87.2	61.1	62.8	60.5	44.6	56.2	53.6

Table 3. Person detection results on the CEPDOF and WEPDToF datasets

Method	CEPDOF							WEPDToF					
	mAP	AP ₅₀	AP ₇₅	Precision	Recall	F1-score	mAP	AP ₅₀	AP ₇₅	Precision	Recall	F1-score	
Seidel <i>et al.</i> [43]	VISAPP'19	20.9	50.6	10.2	80.6	39.5	53.0	16.1	39.4	9.0	70.9	38.6	50.0
Li <i>et al.</i> [25]	AVSS'19	34.2	75.7	28.6	86.3	65.4	74.4	25.2	69.9	30.2	81.4	64.5	72.0
Tamura <i>et al.</i> [50] ¹	WACV'19	28.8	61.6	23.0	73.1	65.8	69.3	12.8	27.2	10.9	53.0	34.3	41.6
RAPiD [10] ¹	CVPRW'20	38.3	78.6	30.8	91.8	80.3	85.7	25.0	54.0	17.4	83.7	57.6	68.2
OARPD [35] ¹	MTA'24	11.4	28.9	6.6	80.5	31.3	45.1	4.1	10.0	2.2	28.8	19.0	22.9
Yang <i>et al.</i> [65] ¹	ICCV'23	39.7	78.3	37.1	82.9	72.6	77.4	20.5	45.3	16.3	66.8	43.0	52.3
Ours		42.8	85.6	38.7	91.8	81.8	86.5	37.5	74.9	34.8	81.7	69.0	74.8

¹ We trained networks for evaluation.**Table 4.** Ablation study on the LOAF test set

Method	mAP	AP ₅₀	AP ₇₅	AP _n	AP _m	AP _f	AP _{seen}	AP _{unseen}
Baseline ¹	40.2	74.0	39.6	48.2	49.5	32.7	42.5	38.7
+ Panorama ²	49.8	84.7	52.7	59.3	55.3	39.7	51.0	48.9
+ PDAT	54.5	87.2	61.1	62.8	60.5	44.6	56.2	53.6

¹ "Baseline" denotes DAB-DETR using fisheye images.² "Panorama" denotes panoramic conversion.**Table 5.** Panoramic-image width analysis on the LOAF test set

Image width	mAP	AP ₅₀	AP ₇₅	AP _n	AP _m	AP _f	AP _{seen}	AP _{unseen}
2048 pixels	47.0	81.3	49.2	58.3	52.0	35.5	48.5	46.0
2560 pixels	51.2	85.1	55.6	61.9	56.4	39.3	53.8	49.7
3072 pixels	54.5	87.2	61.1	62.8	60.5	44.6	56.2	53.6

mean average precision (mAP) following the COCO evaluation [27]. We used the subscripts n , m , and f to denote the near (0–10 m), mid-range (10–20 m), and distant (over 20 m) person positions, respectively, e.g., AP _{n} . LOAF also provides seen and unseen scenes for test splits using the subscripts *seen* and *unseen*, respectively. We used the official splits of the training, validation (val), and test sets.

Results. Our method achieved the highest mAP among the methods listed in Table 2 when used on both the validation and test sets. The mAP obtained using our method was substantially higher than that obtained using Yang *et al.*'s method [65] by values of 5.0 and 8.3 on the LOAF validation and test sets, respectively. In addition, the AP _{f} value obtained using our method on the test set was notably larger than that of Yang *et al.*'s method [65] by 32.0, where 67% of the bounding boxes were labeled as f : over 20 m. Our method also achieved an AP_{*seen*} of 56.2 and an AP_{*unseen*} of 53.6 on the test set, thus outperforming the other methods.

The substantial margin between our method and Yang *et al.*'s method [65] on the unseen test set of 8.7 demonstrates the scene robustness.

4.3.2. Person detection on CEPDOF

Metrics and protocols. CEPDOF [10] provides bounding box annotations without person locations in the world coordinates. Therefore, we evaluated the detection performance using the AP. Similar to prior works [10, 51, 65], we also used precision, recall, and the F1-score. Following the procedure of [65], we trained the method of Tamura *et al.* [50], along with RAPiD [10], OARPD [35], Yang *et al.* [65], and our method, using HABBOF [25] and WEPDToF [51] after pretraining these methods on COCO [27], although MW-R [10] was not used for the training because it is not publicly available.

Results. Our method achieved the highest mAP, AP₅₀, and AP₇₅ values on CEPDOF among the methods listed in Table 3. The mAP, AP₅₀, and AP₇₅ values achieved using our method are higher than those obtained using Yang *et al.*'s method [65] by values of 3.1, 7.3, and 1.6, respectively. Additionally, the F1-score of our method was greater than that of Yang *et al.*'s method [65] by 9.1.

4.3.3. Person detection on WEPDToF

Metrics and protocols. We used the evaluation metrics of CEPDOF, as described in Section 4.3.2. We trained the methods of Tamura *et al.* [50], RAPiD [10], OARPD [35], Yang *et al.* [65], and our method, using HABBOF and CEPDOF after they were pretrained on COCO following [65], although MW-R was again not used for the training because it is not publicly available.

Table 6. Person localization results using position errors (PE) ↓ in meters on the LOAF validation and test sets

Method		val						test					
		mPE	PE _n	PE _m	PE _f	PE _{seen}	PE _{unseen}	mPE	PE _n	PE _m	PE _f	PE _{seen}	PE _{unseen}
Seidel <i>et al.</i> [43]	VISAPP'19	1.298	0.561	1.332	3.109	1.206	1.382	1.321	0.706	1.309	3.482	1.306	1.386
Li <i>et al.</i> [25]	AVSS'19	0.898	0.502	0.871	2.650	0.832	0.962	0.913	0.543	0.884	2.780	0.904	0.998
Tamura <i>et al.</i> [50]	WACV'19	0.755	0.429	0.736	1.862	0.709	0.821	0.778	0.471	0.826	2.160	0.724	0.836
RAPiD [10]	CVPRW'20	0.674	0.426	0.623	1.403	0.625	0.757	0.682	0.461	0.664	1.445	0.638	0.776
OARPD [35]	MTA'24	-	-	-	-	-	-	-	-	-	-	-	-
Yang <i>et al.</i> [65]	ICCV'23	0.368	0.144	0.363	0.775	0.318	0.402	0.374	0.148	0.375	0.819	0.326	0.398
Ours		0.286	0.096	0.182	0.635	0.256	0.306	0.277	0.115	0.261	0.528	0.282	0.274

Results. Similar to the CEPDOF results, our method achieved the highest mAP, AP₅₀, and AP₇₅ results on WEPDFOB among the methods listed in Table 3. The mAP values achieved on CEPDOF using both the conventional methods and our method were larger than those obtained on WEPDFOB because WEPDFOB has more scenes; *i.e.*, WEPDFOB consists of 16 videos, and CEPDOF consists of 8 videos. Comparison between the CEPDOF and WEPDFOB results shows that the methods of Tamura *et al.* [50], RAPiD [10], OARPD [35], and Yang *et al.* [65] apparently require diverse images because the network is trained on fisheye images that include rotated persons.

4.3.4. Diagnostic study

We conducted a diagnostic study on the LOAF test set. Table 4 shows the ablation study results. The baseline represents DAB-DETR [30] with the SG-Former-S [39] for the backbone when using fisheye input images. The second row demonstrates the effectiveness of the panoramic conversion. The panoramic images were suitable for DAB-DETR because they removed the person rotations. After the panoramic conversion was adopted, the performance increased by an mAP of 9.6. We also validated the effectiveness of the PDAT process. The third row indicates that our method using PDAT provided substantially improved person detection results when compared with our method without PDAT by an mAP of 4.7. Therefore, the PDAT alleviated the problems caused by the variations in person size dramatically. Similar to the mAP, the other metrics were improved notably.

In addition, Table 5 shows the dependence of the panoramic image width. The 3072-pixel panoramic image width is suitable for the 1024×1024-pixel fisheye images because the circumference of the fisheye image is $\pi \times 1024 = 3217 \approx 3072$. Therefore, the 3072-pixel image width without shrinkage led to the best performance among the widths of 2048, 2560, and 3072 pixels.

4.3.5. Person localization

Metrics and protocols. To validate the person localization accuracy, we compared our method with the conventional methods. We evaluated the individual person positions from the bounding boxes using Yang *et al.*'s approach [65], as

described in Section 4.2. We used the position error (PE) in meters as the horizontal distance between the ground-truth person position and the person position estimated from the bounding boxes. We also used the same subscripts used in Section 4.3.1, *e.g.*, PE_n. These estimated bounding boxes were the same as the person detection results on LOAF from Section 4.3.1.

Results. Our method achieved the lowest mean PE (mPE), as indicated in Table 6. The mPE for our method is smaller than that of Yang *et al.*'s method [65] on the LOAF test set by 0.097 m. Similar to the person detection performance, our method realized a noteworthy 0.124-m gain in terms of the PE_{unseen} when compared with Yang *et al.*'s method [65]. Our method outperformed the other methods on PE_n, PE_m, and PE_f because of the accuracy of bounding box detection.

5. Conclusion

Limitations. We assume that the fisheye images are stereographic projections. However, this assumption may cause a mismatch with the actual distortion. To address this problem, we will extend our method using deep single image camera calibration techniques [4, 57] that estimate the lens distortion. Another promising direction for future work is to use videos for the input. In this paper, we have focused on person detection and localization from an image.

We have proposed a transformer-based detection and localization method for use with overhead fisheye images. Panoramic remapping and PDAT address person rotation and small-person problems in overhead fisheye images. Our nonuniform tokenization using self-similar figures leverages the significance values to alleviate the imbalance in the significance areas of the feature maps. Experiments demonstrated that our method outperforms the prior methods.

References

- [1] D. Aiger, A. Araujo, and S. Lymen. Yes, we CANN: Constrained approximate nearest neighbors for local feature-based visual localization. In *Proceedings of the IEEE/CVF International Conference on Computer Vision (ICCV)*, pages 13293–13303, 2023. 3

- [2] A. Athwale, A. Afrasiyabi, J. Lagüe, I. Shili, O. Ahmad, and J.-F. Lalonde. DarSwin: Distortion aware radial swin transformer. In *Proceedings of the IEEE/CVF International Conference on Computer Vision (ICCV)*, pages 5906–5915, 2023. 3
- [3] V. Balntas, S. Li, and V. Prisacariu. RelocNet: Continuous metric learning relocalisation using neural nets. In *Proceedings of the European Conference on Computer Vision (ECCV)*, pages 782–799, 2018. 3
- [4] A. P. Dal Cin, F. Azzoni, G. Boracchi, and L. Magri. Revisiting calibration of wide-angle radially symmetric cameras. In *Proceedings of the European Conference on Computer Vision (ECCV)*, page 214–230, 2024. 8
- [5] C. R. del Blanco, P. Carballeira, F. Jaureguizar, and N. García. Robust people indoor localization with omnidirectional cameras using a grid of spatial-aware classifiers. *Signal Processing: Image Communication (SPIC)*, 93:116135, 2021. 2
- [6] C. R. Del-Blanco, P. Carballeira, F. Jaureguizar, and N. García. Robust people indoor localization with omnidirectional cameras using a Grid of Spatial-Aware Classifiers. *Signal Processing: Image Communication (SPIC)*, 93:116135, 2021. 3
- [7] P. Dollár, C. Wojek, B. Schiele, and P. Perona. Pedestrian detection: A benchmark. In *Proceedings of the IEEE Conference on Computer Vision and Pattern Recognition (CVPR)*, pages 304–311, 2009. 1
- [8] X. Dong, J. Bao, D. Chen, W. Zhang, N. Yu, L. Yuan, D. Chen, and B. Guo. CSWin Transformer: A general vision transformer backbone with cross-shaped windows. In *Proceedings of the IEEE/CVF Conference on Computer Vision and Pattern Recognition (CVPR)*, pages 12114–12124, 2022. 3
- [9] A. Dosovitskiy, L. Beyer, A. Kolesnikov, D. Weissenborn, X. Zhai, T. Unterthiner, M. Dehghani, M. Minderer, G. Heigold, S. Gelly, J. Uszkoreit, and N. Houlsby. An image is worth 16x16 words: Transformers for image recognition at scale. In *Proceedings of the International Conference on Learning Representations (ICLR)*, 2021. 3, 5
- [10] Z. Duan, M. Ozan Tezcan, H. Nakamura, P. Ishwar, and J. Konrad. RAPID: Rotation-aware people detection in overhead fisheye images. In *Proceedings of the IEEE/CVF Conference on Computer Vision and Pattern Recognition Workshops (CVPRW)*, pages 2700–2709, 2020. 2, 6, 7, 8
- [11] Z. Fu, Q. Liu, Z. Fu, and Y. Wang. STMTrack: Template-free visual tracking with space-time memory networks. In *Proceedings of the IEEE/CVF Conference on Computer Vision and Pattern Recognition (CVPR)*, pages 13774–13783, 2021. 1
- [12] H. Germain, V. Lepetit, and G. Bourmaud. Neural reprojection error: Merging feature learning and camera pose estimation. In *Proceedings of the IEEE/CVF Conference on Computer Vision and Pattern Recognition (CVPR)*, pages 414–423, 2021. 3
- [13] G. Ghiasi, Y. Cui, A. Srinivas, R. Qian, T.-Y. Lin, E. D. Cubuk, Q. V. Le, and B. Zoph. Simple copy-paste is a strong data augmentation method for instance segmentation. In *Proceedings of the IEEE/CVF Conference on Computer Vision and Pattern Recognition (CVPR)*, pages 2917–2927, 2021. 1, 3
- [14] E. J. Gibson, J. J. Gibson, O. W. Smith, and H. Flock. Motion parallax as a determinant of perceived depth. *Journal of Experimental Psychology*, 58(1):40–51, 1959. 4
- [15] Y. Gong, X. Yu, Y. Ding, X. Peng, J. Zhao, and Z. Han. Effective fusion factor in fpn for tiny object detection. In *Proceedings of the IEEE Winter Conference on Applications of Computer Vision (WACV)*, pages 1159–1167, 2021. 3
- [16] R. Hartley and A. Zisserman. *Multiple View Geometry in Computer Vision*. Cambridge University Press, second edition, 2004. 4
- [17] A. Hassani, S. Walton, J. Li, S. Li, and H. Shi. Neighborhood attention transformer. In *Proceedings of the IEEE/CVF Conference on Computer Vision and Pattern Recognition (CVPR)*, pages 6185–6194, 2023. 3
- [18] S. Huang, Z. Lu, X. Cun, Y. Yu, X. Zhou, and X. Shen. DEIM: DETR with improved matching for fast convergence. In *Proceedings of the IEEE/CVF Conference on Computer Vision and Pattern Recognition (CVPR)*, pages 15162–15171, 2025. 1
- [19] J. Hyeon, J. Kim, and N. Doh. Pose correction for highly accurate visual localization in large-scale indoor spaces. In *Proceedings of the IEEE/CVF International Conference on Computer Vision (ICCV)*, pages 15954–15963, 2021. 3
- [20] H. Ji, Z. Gao, X. Liu, Y. Zhang, and T. Mei. Small object detection leveraging on simultaneous super-resolution. In *Proceedings of the International Conference on Pattern Recognition (ICPR)*, pages 803–810, 2021. 3
- [21] A. Kendall, M. Grimes, and R. Cipolla. PoseNet: A convolutional network for real-time 6-DOF camera relocalization. In *Proceedings of the IEEE International Conference on Computer Vision (ICCV)*, pages 2938–2946, 2015. 3
- [22] A. H. Khan, M. S. Nawaz, and A. Dengel. Localized semantic feature mixers for efficient pedestrian detection in autonomous driving. In *Proceedings of the IEEE/CVF Conference on Computer Vision and Pattern Recognition (CVPR)*, pages 5476–5485, 2023. 1
- [23] A. Krizhevsky, I. Sutskever, and G. E. Hinton. ImageNet classification with deep convolutional neural networks. In *Proceedings of the Advances in Neural Information Processing Systems (NeurIPS)*, 2012. 2
- [24] B.-J. Lee, J. Choi, C. Baek, and B.-T. Zhang. Robust human following by deep bayesian trajectory prediction for home service robots. In *Proceedings of the IEEE International Conference on Robotics and Automation (ICRA)*, pages 7189–7195, 2018. 1
- [25] S. Li, M. Ozan Tezcan, P. Ishwar, and J. Konrad. Supervised people counting using an overhead fisheye camera. In *Proceedings of the IEEE International Conference on Advanced Video and Signal Based Surveillance (AVSS)*, pages 1–8, 2019. 2, 6, 7, 8
- [26] L. Lin, Y. Lu, Y. Pan, and X. Chen. Integrating graph partitioning and matching for trajectory analysis in video surveillance. *IEEE Transactions on Image Processing (TIP)*, 21(12):4844–4857, 2012. 1

- [27] T.-Y. Lin, M. Maire, S. Belongie, J. Hays, P. Perona, D. Ramanan, P. Dollár, and C. L. Zitnick. Microsoft COCO: Common objects in context. In *Proceedings of the European Conference on Computer Vision (ECCV)*, pages 740–755, 2014. 2, 7
- [28] T.-Y. Lin, P. Dollár, R. Girshick, K. He, B. Hariharan, and S. Belongie. Feature pyramid networks for object detection. In *Proceedings of the IEEE Conference on Computer Vision and Pattern Recognition (CVPR)*, pages 936–944, 2017. 2
- [29] K. Liu, Z. Fu, S. Jin, Z. Chen, F. Zhou, R. Jiang, Y. Chen, and J. Ye. ESOD: Efficient small object detection on high-resolution images. *IEEE Transactions on Image Processing (TIP)*, 34:183–195, 2025. 3
- [30] S. Liu, F. Li, H. Zhang, X. Yang, X. Qi, H. Su, J. Zhu, and L. Zhang. DAB-DETR: Dynamic anchor boxes are better queries for DETR. In *Proceedings of the International Conference on Learning Representations (ICLR)*, 2022. 2, 5, 6, 8
- [31] Z. Liu, Y. Lin, Y. Cao, H. Hu, Y. Wei, Z. Zhang, S. Lin, and B. Guo. Swin Transformer: Hierarchical vision transformer using shifted windows. In *Proceedings of the IEEE International Conference on Computer Vision (ICCV)*, pages 9992–10002, 2021. 3, 6
- [32] I. Loshchilov and F. Hutter. Decoupled weight decay regularization. In *Proceedings of the International Conference on Learning Representations (ICLR)*, 2019. 6
- [33] B. Mandelbrot. How long is the coast of britain? statistical self-similarity and fractional dimension. *Science*, 156(3775): 636–638, 1967. 5
- [34] A. Paszke, S. Gross, F. Massa, A. Lerer, J. Bradbury, G. Chanan, T. Killeen, Z. Lin, N. Gimelshein, L. Antiga, A. Desmaison, A. Köpf, E. Yang, Z. DeVito, M. Raison, A. Tejani, S. Chilamkurthy, B. Steiner, L. Fang, J. Bai, and S. Chintala. PyTorch: An imperative style, high-performance deep learning library. In *Proceedings of the Advances in Neural Information Processing Systems (NeurIPS)*, pages 8024–8035, 2019. 6
- [35] R. Qiao, C. Cai, H. Meng, F. Wang, and J. Zhao. OARPD: Occlusion-aware rotated people detection in overhead fish-eye images. *Multimedia Tools and Applications (MTA)*, 83: 90375–90392, 2024. 2, 6, 7, 8
- [36] Y. Rao, W. Zhao, B. Liu, J. Lu, J. Zhou, and C.-J. Hsieh. DynamicViT: Efficient vision transformers with dynamic token sparsification. In *Proceedings of the Advances in Neural Information Processing Systems (NeurIPS)*, pages 13937–13949, 2021. 3
- [37] J. Redmon and A. Farhadi. YOLO9000: Better, faster, stronger. In *Proceedings of the IEEE Conference on Computer Vision and Pattern Recognition (CVPR)*, pages 6517–6525, 2017. 2
- [38] J. Redmon and A. Farhadi. YOLOv3: An incremental improvement. *arXiv preprint arXiv:1804.02767*, 2018. 2
- [39] S. Ren, X. Yang, S. Liu, and X. Wang. SG-Former: Self-guided transformer with evolving token reallocation. In *Proceedings of the IEEE/CVF International Conference on Computer Vision (ICCV)*, pages 5980–5991, 2023. 3, 5, 6, 8
- [40] O. Russakovsky, J. Deng, H. Su, J. Krause, S. Satheesh, S. Ma, Z. Huang, A. Karpathy, A. Khosla, M. Bernstein, A. C. Berg, and L. Fei-Fei. ImageNet large scale visual recognition challenge. *International Journal of Computer Vision (IJCV)*, 115(3):211–252, 2015. 6
- [41] P.-E. Sarlin, C. Cadena, R. Siegwart, and M. Dymczyk. From coarse to fine: Robust hierarchical localization at large scale. In *Proceedings of the IEEE/CVF Conference on Computer Vision and Pattern Recognition (CVPR)*, pages 12708–12717, 2019. 3
- [42] P.-E. Sarlin, A. Unagar, M. Larsson, H. Germain, C. Toft, V. Larsson, M. Pollefeys, V. Lepetit, L. Hammarstrand, F. Kahl, and T. Sattler. Back to the feature: Learning robust camera localization from pixels to pose. In *Proceedings of the IEEE/CVF Conference on Computer Vision and Pattern Recognition (CVPR)*, pages 3246–3256, 2021. 3
- [43] R. Seidel, A. Apitzsch, and G. Hirtz. Improved person detection on omnidirectional images with non-maxima suppression. In *Proceedings of the International Conference on Computer Vision Theory and Applications (VISAPP)*, 2019. 2, 6, 7, 8
- [44] A. Sharma and J. Ventura. Unsupervised learning of depth and ego-motion from cylindrical panoramic video. In *Proceedings of the IEEE International Conference on Artificial Intelligence and Virtual Reality (AIVR)*, pages 58–587, 2019. 5
- [45] J. Shermeyer and A. Van Etten. The effects of super-resolution on object detection performance in satellite imagery. In *Proceedings of the IEEE/CVF Conference on Computer Vision and Pattern Recognition Workshops (CVPRW)*, pages 1432–1441, 2019. 3
- [46] B. Singh and L. S. Davis. An analysis of scale invariance in object detection - SNIP. In *Proceedings of the IEEE/CVF Conference on Computer Vision and Pattern Recognition (CVPR)*, pages 3578–3587, 2018. 3
- [47] B. Singh, M. Najibi, and L. S. Davis. SNIPER: Efficient multi-scale training. In *Proceedings of the Advances in Neural Information Processing Systems (NeurIPS)*, pages 9310–9320, 2018. 3
- [48] H. J. S. Smith. On the integration of discontinuous functions. *Proceedings of the London Mathematical Society*, s1-6(1): 140–153, 1874. 5
- [49] H. Sun, R. Wang, Y. Li, L. Yang, S. Lin, X. Cao, and B. Zhang. SET: Spectral enhancement for tiny object detection. In *Proceedings of the IEEE/CVF Conference on Computer Vision and Pattern Recognition (CVPR)*, pages 4713–4723, 2025. 3
- [50] M. Tamura, S. Horiguchi, and T. Murakami. Omnidirectional pedestrian detection by rotation invariant training. In *Proceedings of the IEEE Winter Conference on Applications of Computer Vision (WACV)*, pages 1989–1998, 2019. 2, 6, 7, 8
- [51] M. O. Tezcan, Z. Duan, M. Cokbas, P. Ishwar, and J. Konrad. WEPDToF: A dataset and benchmark algorithms for in-the-wild people detection and tracking from overhead fish-eye cameras. In *Proceedings of the IEEE/CVF Winter Conference on Applications of Computer Vision (WACV)*, pages 1381–1390, 2022. 2, 6, 7
- [52] A. Torii, H. Taira, J. Sivic, M. Pollefeys, M. Okutomi, T. Pajdla, and T. Sattler. Are large-scale 3D models really nec-

- essary for accurate visual localization? *IEEE Transactions on Pattern Analysis and Machine Intelligence (PAMI)*, 43(3): 814–829, 2021. 3
- [53] Z. Tu, H. Talebi, H. Zhang, F. Yang, P. Milanfar, A. Bovik, and Y. Li. MaxViT: Multi-axis vision transformer. In *Proceedings of the European Conference on Computer Vision (ECCV)*, page 459–479, 2022. 3
- [54] F. Ö. Ünel, B. O. Özkalayci, and C. Çiğla. The power of tiling for small object detection. In *Proceedings of the IEEE/CVF Conference on Computer Vision and Pattern Recognition Workshops (CVPRW)*, pages 582–591, 2019. 3
- [55] R. Varghese and S. M. YOLOv8: A novel object detection algorithm with enhanced performance and robustness. In *Proceedings of the International Conference on Advances in Data Engineering and Intelligent Computing Systems (ADICS)*, pages 1–6, 2024. 2
- [56] A. Vaswani, N. Shazeer, N. Parmar, J. Uszkoreit, L. Jones, A. N. Gomez, Ł. Kaiser, and I. Polosukhin. Attention is all you need. In *Proceedings of the Advances in Neural Information Processing Systems (NeurIPS)*, pages 6000–6010, 2017. 2
- [57] N. Wakai, S. Sato, Y. Ishii, and T. Yamashita. Rethinking generic camera models for deep single image camera calibration to recover rotation and fisheye distortion. In *Proceedings of the European Conference on Computer Vision (ECCV)*, pages 679–698, 2022. 5, 8
- [58] F. Walch, C. Hazirbas, L. Leal-Taixe, T. Sattler, S. Hilsenbeck, and D. Cremers. Image-based localization using LSTMs for structured feature correlation. In *Proceedings of the IEEE International Conference on Computer Vision (ICCV)*, pages 627–637, 2017. 3
- [59] J. Wang, K. Sun, T. Cheng, B. Jiang, C. Deng, Y. Zhao, D. Liu, Y. Mu, M. Tan, X. Wang, W. Liu, and B. Xiao. Deep high-resolution representation learning for visual recognition. *IEEE Transactions on Pattern Analysis and Machine Intelligence (PAMI)*, 43(10):3349–3364, 2021. 3
- [60] W. Wang, J. Dai, Z. Chen, Z. Huang, Z. Li, X. Zhu, X. Hu, T. Lu, L. Lu, H. Li, X. Wang, and Y. Qiao. InternImage: Exploring large-scale vision foundation models with deformable convolutions. In *Proceedings of the IEEE/CVF Conference on Computer Vision and Pattern Recognition (CVPR)*, pages 14408–14419, 2023. 1
- [61] W. Wang, W. Chen, Q. Qiu, L. Chen, B. Wu, B. Lin, X. He, and W. Liu. CrossFormer++: A versatile vision transformer hinging on cross-scale attention. *IEEE Transactions on Pattern Analysis and Machine Intelligence (PAMI)*, 46(5): 3123–3136, 2024. 3
- [62] Z. Xia, X. Pan, S. Song, L. E. Li, and G. Huang. Vision transformer with deformable attention. In *Proceedings of the IEEE/CVF Conference on Computer Vision and Pattern Recognition (CVPR)*, pages 4784–4793, 2022. 3
- [63] Y. Xie, L. Lin, and Y. Jia. Tracking objects with adaptive feature patches for PTZ camera visual surveillance. In *Proceedings of the International Conference on Pattern Recognition (ICPR)*, pages 1739–1742, 2010. 1
- [64] L. Yang, Z. Bai, C. Tang, H. Li, Y. Furukawa, and P. Tan. SANet: Scene agnostic network for camera localization. In *Proceedings of the IEEE/CVF International Conference on Computer Vision (ICCV)*, pages 42–51, 2019. 3
- [65] L. Yang, L. Li, X. Xin, Y. Sun, Q. Song, and W. Wang. Large-scale person detection and localization using overhead fisheye cameras. In *Proceedings of the IEEE/CVF International Conference on Computer Vision (ICCV)*, pages 19904–19914, 2023. 1, 2, 3, 5, 6, 7, 8
- [66] T. Yoshimi, M. Nishiyama, T. Sonoura, H. Nakamoto, S. Tokura, H. Sato, F. Ozaki, N. Matsuhira, and H. Mizoguchi. Development of a person following robot with vision based target detection. In *Proceedings of the IEEE/RSJ International Conference on Intelligent Robots and Systems (IROS)*, pages 5286–5291, 2006. 1
- [67] X. Yu, Y. Gong, N. Jiang, Q. Ye, and Z. Han. Scale match for tiny person detection. In *Proceedings of the IEEE Winter Conference on Applications of Computer Vision (WACV)*, pages 1246–1254, 2020. 3
- [68] T. Yuan, X. Zhang, K. Liu, B. Liu, C. Chen, J. Jin, and Z. Jiao. Towards surveillance video-and-language understanding: New dataset, baselines, and challenges. In *Proceedings of the IEEE/CVF Conference on Computer Vision and Pattern Recognition (CVPR)*, pages 22052–22061, 2024. 1
- [69] C.-B. Zhang, Y. Zhong, and K. Han. Mr. DETR: Instructive multi-route training for detection transformers. In *Proceedings of the IEEE/CVF Conference on Computer Vision and Pattern Recognition (CVPR)*, pages 9933–9943, 2025. 1
- [70] D. Zhang, L. Birner, F. Pancheri, C. Rehekampff, D. Burschka, and T. C. Lueth. A hybrid human tracking system using UWB sensors and monocular visual data fusion for human following robots. In *Proceedings of the IEEE/RSJ International Conference on Intelligent Robots and Systems (IROS)*, pages 10878–10883, 2024. 1
- [71] S. Zhang, R. Benenson, M. Omran, J. Hosang, and B. Schiele. Towards reaching human performance in pedestrian detection. *IEEE Transactions on Pattern Analysis and Machine Intelligence (PAMI)*, 40(4):973–986, 2018. 1
- [72] J. Zhu, J. Zhu, X. Wan, C. Wu, and C. Xu. Object detection and localization in 3D environment by fusing raw fisheye image and attitude data. *Journal of Visual Communication and Image Representation (JVCIR)*, 59:128–139, 2019. 3
- [73] L. Zhu, X. Wang, Z. Ke, W. Zhang, and R. Lau. BiFormer: Vision transformer with bi-level routing attention. In *Proceedings of the IEEE/CVF Conference on Computer Vision and Pattern Recognition (CVPR)*, pages 10323–10333, 2023. 3
- [74] P. Zhu, L. Wen, X. Bian, H. Ling, and Q. Hu. Vision meets drones: A challenge. *arXiv preprint arXiv:1804.07437*, 2018. 2
- [75] Z. Zong, G. Song, and Y. Liu. DETRs with collaborative hybrid assignments training. In *Proceedings of the IEEE/CVF International Conference on Computer Vision (ICCV)*, pages 6725–6735, 2023. 1